J. Electroanal. Chem., 215 (1986) 317–329
Elsevier Sequoia S.A., Lausanne – Printed in The Netherlands

ELECTROCHEMICAL FACETING OF POLYCRYSTALLINE GOLD IN 1 *M* H_2SO_4

C.L. PERDRIEL and A.J. ARVIA

*Instituto de Investigaciones Fisicoquímicas Teóricas y Aplicadas (INIFTA *), Casilla de Correo 16, Sucursal 4, (1900) La Plata (Argentina)*

M. IPOHORSKI

Departamento de Materiales, Comisión Nacional de Energía Atómica, Buenos Aires (Argentina)

(Received 10th April 1986; in revised from 23rd June 1986)

ABSTRACT

Electrochemical faceting of polycrystalline (pc) gold electrodes in 1 *M* H_2SO_4 was investigated by employing wire and bead-shaped electrodes. Electrochemical faceting was produced by applying a repetitive symmetrical square wave potential signal in the 2–4 kHz range and upper and lower potential limits ranging between 1.44 and 1.60 V (vs. RHE) and 0.10 and 1.10 V, respectively. The degree of faceting was followed voltammetrically principally through the O-electroadsorption/electrodesorption process. Electrochemical information was complemented with scanning electron microscopic observations. The results are discussed in terms of the equilibrium potential of reactions involving different gold species, and the potential of zero charge, hydrophobicity and anion adsorbability of the (110), (100) and (111) crystallographic faces of gold. The kinetics of electrochemical faceting of gold can be explained through the two-stage mechanism proposed earlier for polycrystalline platinum in acid electrolyte.

INTRODUCTION

Observations of electrochemical faceting of gold and platinum electrodes produced through successive electrooxidation/electroreduction cycles have been reported by different authors for nearly two decades [1–4]. For single-crystal gold electrodes, faceting implies a slight decrease in crystallographic orientation [3], and in this case adsorption and desorption processes play an important role in the modification of surface microgeometry.

Recently electrochemical faceting was investigated more extensively for different solid metal electrodes by employing either single-crystal or polycrystalline electrodes

* Facultad de Ciencias Exactas, Universidad Nacional de La Plata.

in order to learn about the kinetics and mechanism of the process and the conditions needed to achieve reproducible electrode surfaces both in terms of orientation and roughness [5–13]. In this direction, several electrochemical procedures were developed recently for producing electrochemical faceting at metal electrode surfaces through the application of relatively fast periodic potential perturbations covering a certain preset range of potentials and frequencies [5–7,10,12,13]. One of these procedures [5,6,10] consists in the application of a square wave potential function at frequencies of the order of 1 kHz or more within the potential range of H- and O-adatom electroadsorption and electrodesorption at the submonolayer or monolayer level. This procedure was applied to promote (100), (110) and (111) faceting of polycrystalline and single-crystal platinum specimens. In this case, the extent of faceting was followed through the voltammetric response of the H-adatom electroadsorption/electrodesorption reactions in acid electrolytes, scanning electron microscopy [12,13] and electron tunnelling microscopy [14].

The present paper deals with the investigation of electrochemical faceting of polycrystalline gold in acid electrolytes. Surface changes are followed principally through the voltammetric response of the O-adatom electroadsorption. Occasionally, underpotential deposition of lead on the faceted gold surface is also made. In recent years, the surface reactions of O and Pb atoms on gold single-crystal electrodes were investigated [15,16]. This renders, in principle, the possibility of comparing the electrochemical behaviour of faceted gold electrode surfaces with those of different gold single-crystal electrodes. The electrochemical measurements are complemented with scanning electron microscopic observations.

EXPERIMENTAL

Two different types of gold working electrodes were used; namely, polycrystalline wires (Engelhard, 99.99% purity), which were mirror polished with alumina powder (0.3 μm particle diameter), etched in a sulphuric acid + nitric acid mixture and rinsed repeatedly in triply distilled water, and bead-type electrodes shaped by melting the extreme of a piece of gold wire in a small oxygen/gas torch flame and finally potential cycled in 1 M H_2SO_4 at 0.1 V/s between -0.1 and 1.70 V (vs. RHE) to obtain a voltammogram which was reproducible to better than 1% between successive cycles. Bead-type electrodes are particularly useful for determining the influence of the electrode geometry and thermal treatment and to avoid field point effects on the electrochemical faceting. In addition, bead-type electrodes offer the possibility of working with a polycrystalline (pc) specimen containing only either a few crystallographic grains or eventually a single crystal. The potential of the working electrode was measured against a static hydrogen electrode in the acid electrolyte (1 M H_2SO_4). The counter-electrode was a large-area gold sheet surrounding the working electrode symmetrically. The electrolyte solution was 1 M H_2SO_4 prepared from Merck a.r. 98% H_2SO_4 and MilliQ# water.

Electrochemical faceting was carried out at 25 °C by using a symmetric repetitive square wave potential signal (RSWPS) at the frequency f between the potentials E_1

and E_u in the following ranges: $0.10\ V \leqslant E_l \leqslant 1.15\ V$; $1.44 \leqslant E_u \leqslant 1.60$; $2\ kHz \leqslant f \leqslant 4\ kHz$. The duration of the RSWPS, t, was varied between 5 min and 20 h. The preferentially oriented gold surface was followed through the voltammetric response of the O-electroadsorption reaction, at 0.1 V/s in the 0.00–1.70 V range. Occasionally, voltammograms for upd of lead in 10^{-2} *M* $HClO_4 + 10^{-3}$ *M* $Pb(ClO_4)_2$ were obtained at 0.01 V/s, in the range −0.10 to 0.65 V. The electrochemical measurements were complemented with SEM observations, taken after keeping the specimens in a clean air atmosphere for a certain time after the electrochemical runs.

RESULTS

The voltammogram of a bright pc gold electrode, either wire or bead, in 1 *M* H_2SO_4 without electrochemical faceting (blank) (Fig. 1a) exhibits a multiplicity of anodic peaks in the 1.40–1.70 V range related to the electroformation of O-containing species and a sharp cathodic peak with a small shoulder at its negative potential side, both related to the complementary O-electroreduction process. The voltammogram also shows a relatively large potential window extending from 0.00 to 1.00 V which is in the potential range usually denoted as the non-faradaic (double layer) region. The SEM patterns of both the bead-type and the polished electrode surface (Figs. 2a and 2b) show randomly distributed irregularities.

On the other hand, the voltammogram resulting after the electrochemical faceting produced by a RSWPS between $E_l = 0.50$ V and $E_u = 1.60$ V at $f = 2.0$ kHz, in the same electrolyte (Fig. 1a), shows a substantial change in the structure of the complex anodic peak as compared to that described previously. The new voltammo-

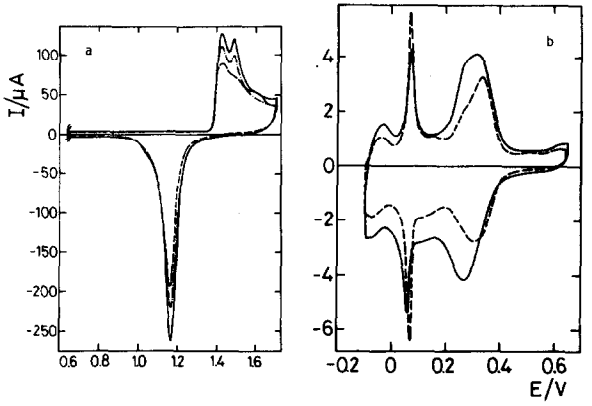

Fig. 1. (a) Voltammograms run at 0.1 V/s in 1 *M* H_2SO_4 at 25°C. (———) After 1 h RSWPS at 2.00 kHz between 0.50 and 1.60 V; (— · —) after 15 min RSWPS at 2.00 kHz between 0.50 and 1.60 V; (– – –) bead-shaped pc gold. (b) Voltammograms run at 0.010 V/s in 10^{-2} *M* $HClO_4$ and 10^{-3} *M* $Pb(ClO_4)_2$. (– – –) Bead-shaped pc gold; (———) after 3.15 h RSWPS at 2.00 kHz between 0.50 and 1.60 V. The potentials are referred to a RHE in 1 *M* $HClO_4$.

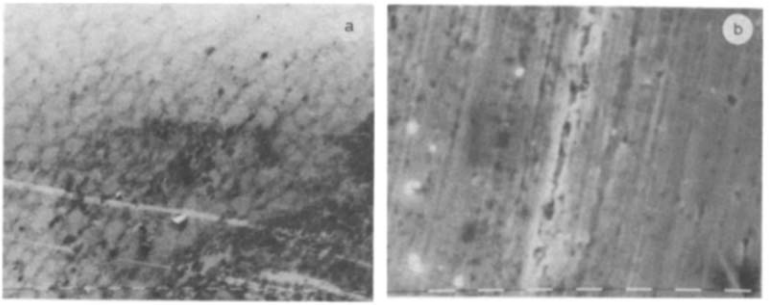

Fig. 2. SEM micrographs. (a) Untreated bead-shaped pc gold. 1600×(1 μm). (b) Untreated polished pc wire gold. 3200×(1 μm).

gram has two distinguishable peaks, one at 1.43 V (peak I-O) and the other at 1.49 V (peak II-O), and there is a considerable increase of both the anodic and the cathodic voltammetric charge (by a factor of about 1.5) after 3 h RSWPS, although the anodic to cathodic charge ratio remains equal to one. The first voltammetric cycles at a low sweep rate (< 0.1 V/s) show a slight decrease in the height of peak I-O, although the stabilized voltammogram is practically attained after the fourth cycle. These voltammetric changes become more remarkable on extending the duration of the RSWPS treatment. Likewise, comparable voltammetric changes are obtained for the upd of lead (Fig. 1b). In this case, the blank exhibits a pair of conjugated sharp peaks (I-Pb) at 0.065 V and a second pair of broad peaks (II-Pb) at 0.34 V. After the RSWPS treatment a decrease in the height of peak I-Pb and a substantial increase in that of peak II-Pb are noticed. As for the O-electroformation/electroreduction voltammogram, in this case the entire voltammetric charge also increases according to the duration of the RSWPS treatment. Similar voltammetric responses are obtained for $f = 3$ and 4 kHz.

The voltammogram depicted in Fig. 1a is similar to that described for the Au (110) plane in 0.5 M H_2SO_4 at 0.070 V/s at 30°C [17]. A similar correspondence also appears concerning the voltammetric stabilization under repetitive triangular potential scanning at 0.1 V/s [17], although in the present case the relative changes in height of peaks I-O and II-O on potential cycling operate in the reverse direction. Likewise, the voltammetric changes in upd lead resulting from untreated and faceted gold electrodes occur in the same direction as those shown recently for the Au (110) plane [18,19].

After electrochemical faceting for 3 h at 2 kHz between $E_l = 0.50$ V and $E_u = 1.60$ V, the gold wire portion offers a clear grain structure with straight line grain boundaries (Fig. 3a). The grain size, although variable, can be estimated to be of the order of 0.01 mm^2. The surface of each grain involves a porous structure made up of parallel steps (Fig. 3b). The electrochemical faceting depends exclusively on the preset potential perturbation parameters and becomes independent of the preparation of the gold electrode. The gold bead portion containing a few crystallo-

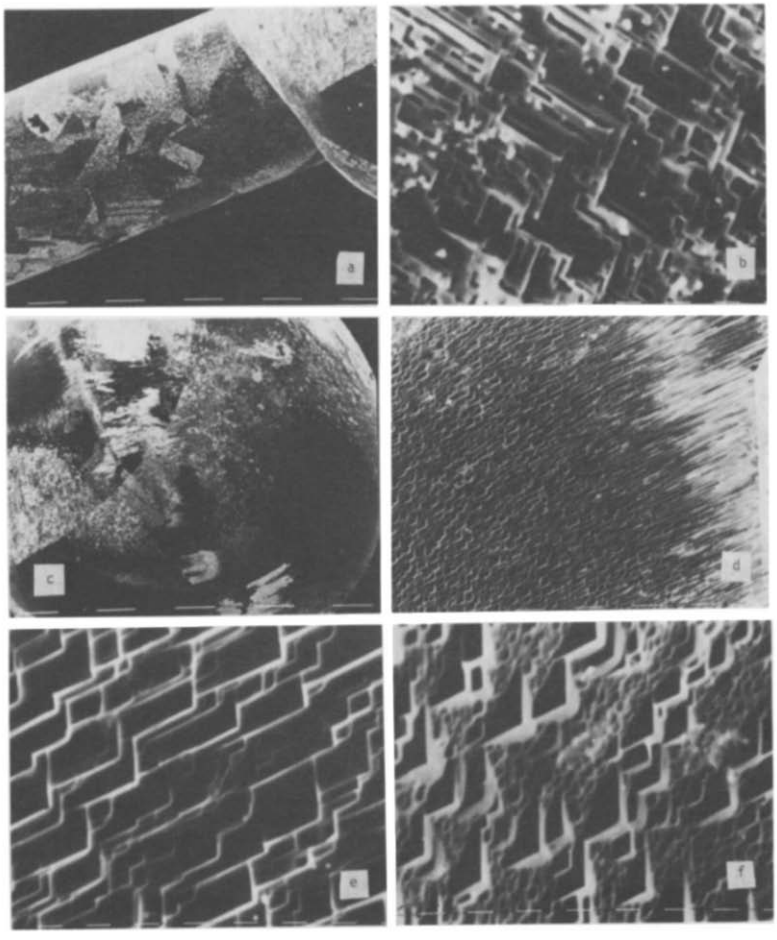

Fig. 3. SEM micrographs. Bead-shaped pc gold after 3 h 10 min RSWPS at 2.00 kHz between 0.50 and 1.60 V. (a) 50×(100 μm); (b) 3200×(1 μm); (c) 50×(100 μm); (d) 400×(10 μm); (e) 3200×(1 μm), (f) 3200×(1 μm).

graphic grains (Fig. 3c) reveals a complex distribution of crystallographic poles [20], and shows the development of a surface with the preferred crystallographic orientation, varying from a nearly right-angled pattern to a parallel channel-like configuration (Fig. 3d). At certain regions, the density of the right-angled steps decreases and the roughness of the electrode surface increases (Figs. 3e–3f).

For $E_l = 0.1$ V, $E_u = 1.60$ V and $f = 2.94$ kHz, the voltammogram resulting after the RSWPS (Figs. 4a and 4b) exhibits an increase in both the voltammetric charge and the height of peak I-O, as one should expect for the latter in the development of a (100)-type preferred orientation. After applying a RSWPS for 17.5 h, the peak I-O becomes sharp and the charge increases by a factor of 3.5. For this long lasting run,

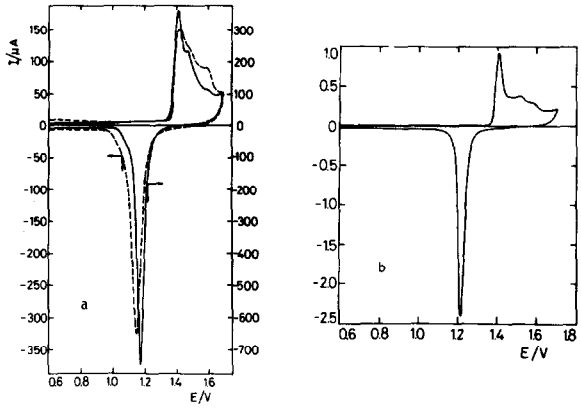

Fig. 4. Voltammograms run at 0.1 V/s in 1 *M* H_2SO_4 at 25°C. (a) (———) After 3 h RSWPS at 4.00 kHz between 0.10 and 1.60 V; (– – –) untreated polished pc gold. (b) (———) After 17.5 h RSWPS at 4.00 kHz between 0.10 and 1.60 V.

the SEM micrograph of the electrode surface corresponds to that of a crystalline metal powder (Fig. 5). In this case, it was further observed that the wall of the glass cell containing the electrolyte from previous voltammetric runs as well as the immersed electrode was covered by a thin gold mirror, and a soluble Au(III) species in the electrolyte was detected by the *o*-tolidine assay [21,22]. The voltammetric response of RSWPS-treated electrodes was also followed in 1 *M* $HClO_4$ at 0.010 and 0.020 V/s to compare their voltammetric behaviour to that of Au single-crystal electrodes previously reported by other authors [23,24]. The RSWPS-treated gold electrodes exhibit three anodic peaks at 1.44, 1.48 and 1.55 V, respectively, although their relative heights are very sensitive to the voltammetric sweep rate (Fig. 6), which suggests the development of a stable (100)-type preferred orientation.

Finally, for $E_l = 0.80$ V, $E_u = 1.60$ V and f between 3 and 4 kHz, a different distribution of the anodic voltammetric peaks is observed (Fig. 7), with a prevalence

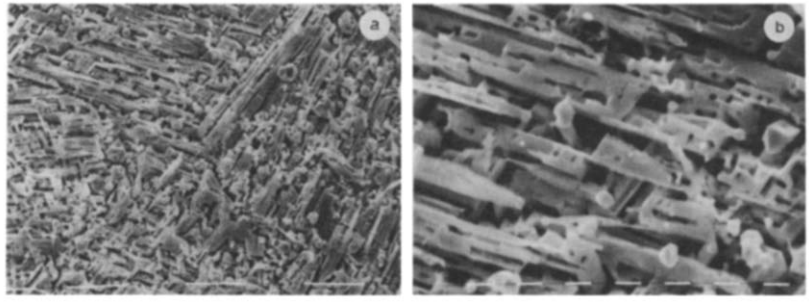

Fig. 5. SEM micrographs. Polished gold after 17.5 h RSWPS at 4.00 kHz between 0.10 and 1.60 V. (a) 800×(10 μm); (b) 3200×(1 μm).

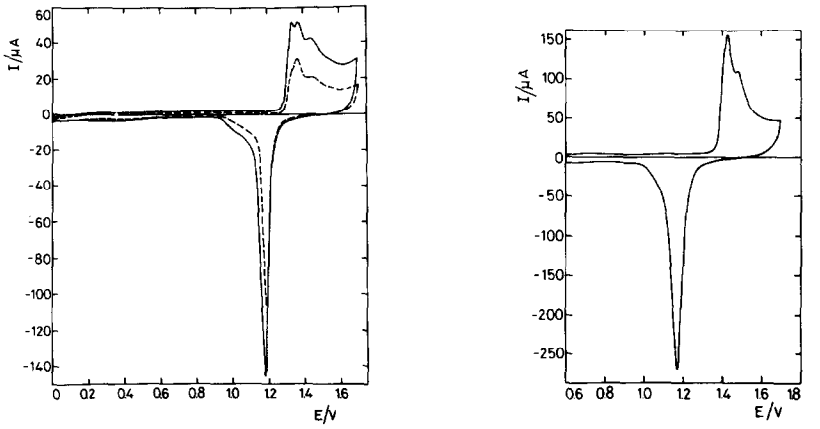

Fig. 6. Voltammograms run in 1 *M* $HClO_4$ at 25°C, after 17.5 h RSWPS at 4.00 kHz between 0.10 and 1.60 V. (– – –) At 0.010 V/s; (———) at 0.020 V/s. The potentials are referred to a RHE in 1 *M* $HClO_4$.

Fig. 7. Voltammograms run at 0.10 V/s in 1 *M* H_2SO_4 at 25°C. Polished gold after 2.8 h RSWPS at 3.00 kHz between 0.8 and 1.60 V.

of peaks at 1.43 V, a shoulder at the upper potential side and a relatively large increase in the voltammetric charge. The voltammogram depicted in Fig. 7 can be changed in the direction of the height increase of peak II-O by decreasing E_l to 0.50 V. A better resolution of peak II-O can be accomplished by potential cycling at 0.1 V/s in 1 *M* H_2SO_4. The corresponding SEM patterns show at the centre of each crystallographic pole a spike-like configuration (Fig. 8a) surrounded by an apparent flat crown region which continues with stepped channel-like arrangements in some regions and a spike-like pit configuration in others. The grain boundaries exhibit a clear faceting transition (Fig. 8b). For $E_u = 1.60$ V, some regions of the surface of

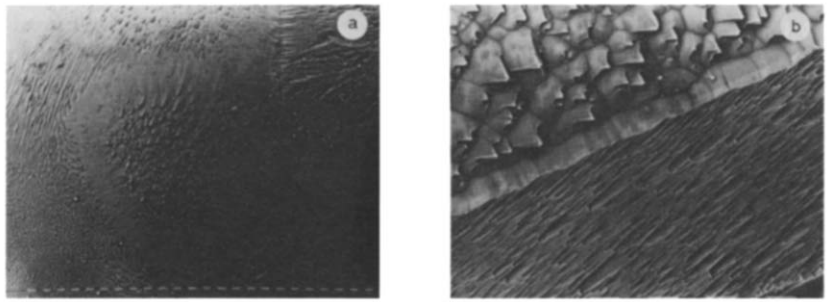

Fig. 8. SEM micrographs. Bead-shaped gold after 13 h RSWPS at 2.5 kHz between 0.8 and 1.60 V. (a) 100×(10 μm); (b) 400×(10 μm).

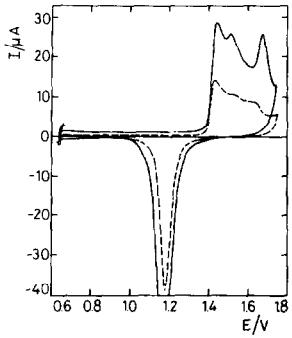

Fig. 9. Voltammograms run at 0.10 V/s in 1 *M* H_2SO_4 at 25°C. (– – –) Untreated bead-shaped; (———) after 20.4 h RSWPS at 2.94 kHz between 0.50 and 1.44 V.

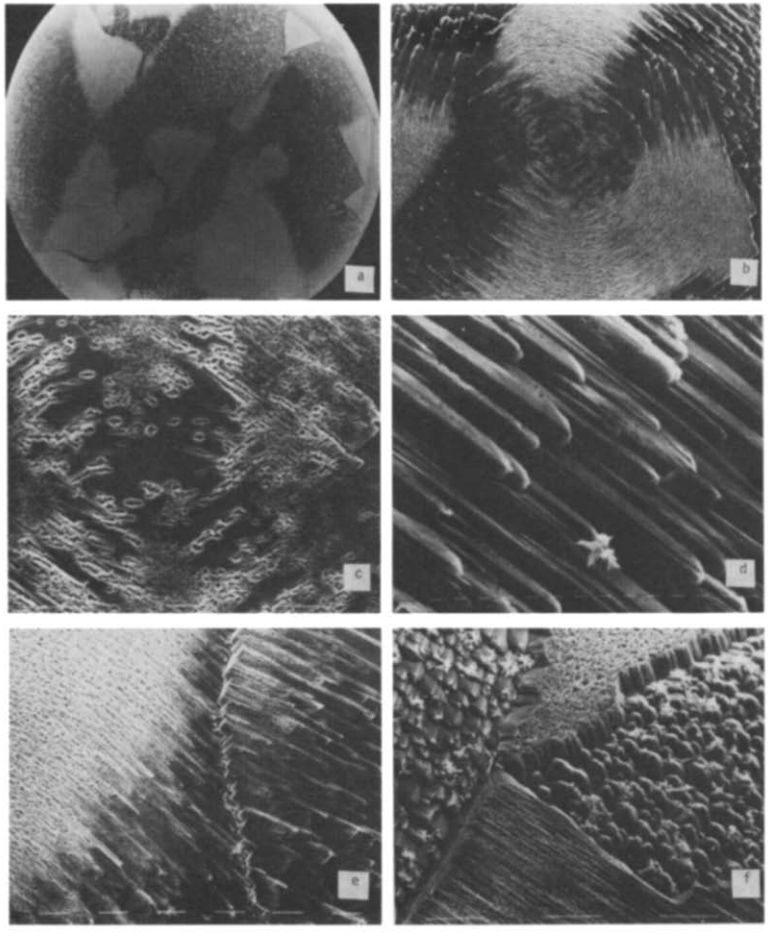

Fig. 10. SEM micrographs. Bead-shaped gold after 20.4 h RSWPS at 2.94 kHz between 0.5 and 1.44 V. (a) 100×(100 μm); (b) 200×(10 μ); (c) 800×(10 μm); (d) 1600×(1 μm); (e) 400×(10 μm); (f) 800×(10 μm).

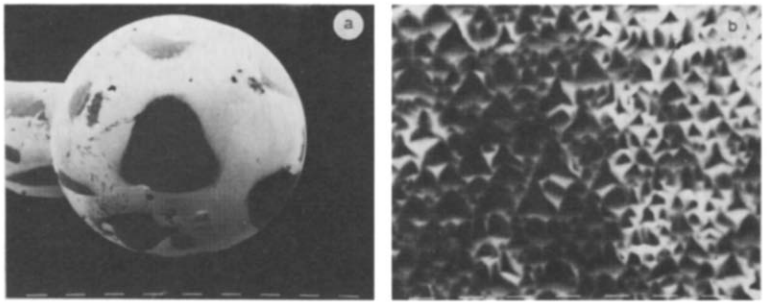

Fig. 11. SEM micrographs. Bead-shaped gold after 2 h at 2.94 kHz between 0.10 and 1.47 V. (a) 25×(100 μm); (b) 3200×(1 μm).

the borders of the repeating geometric figures become less clear than in those runs involving lower E_u values. This effect is presumably caused by the incomplete electroreduction of the surface oxide produced at the relatively high E_u value.

By changing the electrochemical faceting conditions to $E_l = 0.50$ V, $E_u = 1.44$ V and $f = 2.94$ kHz after 20.4 h, the subsequent voltammogram at 0.1 V/s in 1 *M* H_2SO_4 (Fig. 9) exhibits peaks I-O, II-O and III-O, with a remarkable relative increase in the definition and charge of peak III-O located at 1.66 V. This voltammogram suggests the development of a (111)-type preferred orientation [3,23]. The resulting surface structure appears rather unstable to potential cycling as compared to those described previously, since the three peaks decrease during the potential cycling at 0.1 V/s. The corresponding SEM patterns after 20 h of RSWPS treatment develop an interesting faceting (Fig. 10a). Around each crystallographic pole (Figs. 10b and 10c) channel-like and spike-like configurations can be distinguished together with abrupt transitions at grain boundaries (Figs. 10e–10f).

On the other hand, after 2 h of RSWPS treatment at $f = 2.94$ kHz, $E_l = 0.1$ V and $E_u = 1.47$ V, the SEM low magnification pattern exhibits a distribution of crystallographic poles at the few grains (Fig. 11a). At higher magnifications spike-like arrangements involving chains of similarly oriented tetrahedra sharing two opposite corners can be clearly seen (Fig. 11b). The voltammogram corresponding to this type of gold electrode is similar to that depicted in Fig. 4a, where the height of peak I-O is appreciably enhanced.

DISCUSSION

The electrochemical faceting of polycrystalline gold in acid promoted by applying a relatively fast symmetric periodic potential perturbation appears very clearly through SEM patterns and also reflects on the voltammetric O-electroadsorption processes. It is also seen that electrofaceting of gold implies an appreciable increase in the electrode roughness. It should be emphasized that the voltammetric response of gold electrodes is extremely sensitive to the potential perturbation conditions even at the low potential sweep rates usually employed in voltammetry [17,25,26].

The electrochemical faceting of gold and platinum in acid is to a large extent similar, except for the fact that the roughening effects in gold are more remarkable than those in platinum. For f values of the order of 1 kHz, the characteristics of the resulting voltammogram in the O-electroadsorption range are very sensitive to E_l and E_u. Thus, for $E_l = 0.1$ V and $E_u = 1.6$ V, the voltammograms indicate that the (100)-type oriented gold is favoured; for $E_l = 0.5$ V and $E_u = 1.6$ V, the (110)-type oriented gold is apparently the most important; and for $E_l = 0.5$ V and $E_u = 1.44$ V, the (111)-type oriented gold is produced together with other low-index planes. The appearance of (100)- and (111)-type oriented gold is seen more clearly after relatively prolonged electrochemical faceting and is associated with a substantial increase in the voltammetric charge. Likewise, the development of (110)- and (100)-type oriented gold is related to the electrode surfaces which furnish stable voltammograms. This does not seem to be the case for the contribution of the (111)-type preferred orientation.

According to the mechanism recently proposed for platinum [9], electrofaceting of gold should also involve an initiation and a propagation stage. The initiation stage should comprise the electroadsorption of water on gold yielding adsorbed OH species, a reaction which occurs as a relatively fast reversible process at 1.52 V [27,28]. The average half-life-time of adsorbed OH on gold was estimated as ca. 10^{-3} s. This figure correlates with the frequency of the periodic potential perturbation required to promote electrochemical faceting. The propagation stage explains the development of electrofaceting at the multilayer level. It comprises the electroformation of an oxide layer during the anodic half-cycle of the periodic perturbation together with soluble Au species, and during the cathodic half-cycle the electroreduction of the oxide layer and the electrodeposition of soluble Au species. The electrodissolution and electrodeposition of gold correspond to non-symmetric selective reactions depending on the crystallographic characteristics of each portion of the pc metal. The selectiveness of these processes is determined by the fact that for a very thin diffusional layer, which is estimated as 10^{-5} cm for a frequency value of 2 kHz and a diffusion coefficient for the soluble gold species of 10^{-6} cm^2/s, the electrochemical reactions become activation-controlled and practically independent of the ambient phase. Therefore, the preferred electrodeposition yielding a faceting effect covers an average size of the order of μm, as can be seen from the SEM patterns. The formation of soluble gold species during the potential cycling of gold electrodes in acid has already been demonstrated by RDE, thin cell layer voltammetry and chemical analysis [29–31].

The values of E_u and E_l for producing the electrochemical faceting are always more positive and more negative, respectively, than the equilibrium potential values of reactions (2), (4), (6)–(9) and (11) in Table 1. It should be noted that in this respect the equilibrium potentials should be taken only as tentative indications of the potential ranges for the different reactions because under the electrochemical faceting conditions it is likely that the actual potentials operating on the reactions are shifted considerably from the equilibrium values. Likewise, for the symmetric periodic potential perturbation, the average potential is always more negative than

TABLE 1

Equilibrium potentials of the reactions of interest for the electrochemical faceting of gold

Half reaction	$E°/V$	$E°'/V$	Reference
(1) $Au^+ + e^- \rightarrow Au$	1.83		32
(2) $Au(OH)_{ad} + H^+ + e^- \rightarrow Au + H_2O$		1.52	27
(3) $Au(OH) + H^+ + e^- \rightarrow Au + H_2O$	2.33		42
(4) $AuO + 2\,H^+ + 2\,e^- \rightarrow Au + H_2O$	1.37		42
(5) $Au(OH)_2 + 2\,H^+ + 2\,e^- \rightarrow Au + 2\,H_2O$	2.01		42
(6) $Au^{3+} + 3\,e^- \rightarrow Au$	1.52		32
(7) $Au_2O_3(s) + 6\,H^+ + 6\,e^- \rightarrow 2\,Au + 3\,H_2O$	1.51	1.36	42
(8) $Au(OH)_3 + 3\,H^+ + 3\,e^- \rightarrow Au + 3\,H_2O$	1.45		42
(9) $H_3AuO_3 + 3\,H^+ + 3\,e^- \rightarrow Au + 3\,H_2O$	1.56		42
(10) $AuO_2 + 4\,H^+ + 4\,e^- \rightarrow Au + 2\,H_2O$	1.75		42
(11) $Au^{3+} + 2\,e^- \rightarrow Au^+$	1.36		32

any of the values assembled in Table 1. Therefore, for $E_l < 1.15$ V it is reasonable that during the potential cycling no oxide accumulation, and consequently no progressive passivation of the electrode, should be expected, whereas for $E_l = 1.15$ and $E_u = 1.60$ V, as the average applied potential is very close to that of eqn. (7) in Table 1, the accumulation of oxide species becomes possible.

The surface of the pc gold electrode consists of a large number of grains of different types, the complicated surface topography resulting from grain boundaries and other defects. This renders difficult and uncertain any model for describing the physico-chemical characteristics of the crystallographically non-uniform pc surface. Nevertheless, some correlations become useful in attempting to explain the electrochemical faceting of gold in a particular direction. For this purpose, one can assume that the starting surface consists of a certain distribution of the three simplest index faces interacting with water and anions. In the case of gold, it has been clearly determined that the potential of zero charge of the different faces increases according to the following sequence: (110) < (100) < (111) [33]. In addition, in terms of hydrophilicity, the water–gold interaction decreases in the sequence (110) > (100) > (111) [34], and the specific adsorption of anions decreases in the sequence (111) > (100) > (110), as particularly established from the co-adsorption of sulphate ions and pyridine [35]. These data point out the difference in surface energy of the crystal faces that presumably assist the preferred orientation. In this case, the development of (100)- and (110)-type oriented gold apparently involves the greater electrodissolution of the most dense face probably assisted by anion adsorption, as recently discussed for the palladium electrode [36], and the most efficient electrodeposition of the less dense face, to which the greatest metal–water interaction has been assigned.

On the other hand, the prevalence of (110)-type oriented gold can also be thought of in terms of a probable surface reconstruction during electrochemical faceting. From the capacity–potential curves of single-crystal gold–aqueous solution interphases [37] it was concluded that a surface reconstruction exists for the three

low-index gold faces, as was previously observed in ultrahigh vacuum studies of gold single-crystal surfaces [38–41]. The overall electrochemical process yields a surface consisting of a corrugated topography. Results obtained from bead-type electrodes involving only a few faceted grains show clear regions where there is a systematic change in the step and terrace structure along the zones between the low-index corners of the stereographic triangle [20].

The development of voltammetric characteristics corresponding to (111)-type oriented gold requires $E_u = 1.44$ V and very prolonged RSWPS treatment. At this low value of E_u it is rather unlikely that the (111)-type crystallographic faces participate in the redox cycles during the RSWPS treatment since the corresponding O-electroadsorption peak is located at 1.7 V. Hence, the appearance of a contribution of the (111)-type preferred orientation should result from the proper selective electrochemical surface etching produced through the RSWPS. In addition, it is also possible that metallic gold formation at the electrode surface takes place through a disproportionation of Au(I) soluble species generated during the RSWPS treatment. Both processes should be responsible for the relatively large increase in voltammetric area associated with this type of crystallographic orientation.

On the other hand, the strong anion adsorption interaction at certain sites promotes a localized corrosion which also contributes to the increase in electrode roughness. Therefore, despite the fact that the behaviour of gold electrodes is complicated by various concurrent phenomena which are not completely understood at the present time, the electrochemical faceting of gold with the development of a preferred orientation is consistent with the electroadsorption-selective electrodissolution and electrodeposition mechanism discussed recently [8,9].

ACKNOWLEDGEMENTS

This research project was supported financially by the Universidad Nacional de La Plata, the Consejo Nacional de Investigaciones Cientificas y Técnicas and the Comisión de Investigaciones Cientificas de la Provincia de Buenos Aires.

REFERENCES

1 T. Biegler, J. Electrochem. Soc., 114 (1967) 1261.
2 T. Biegler, J. Electrochem. Soc., 116 (1969) 1131.
3 M. Sotto, A. Hamelin and G. Valette, C.R. Acad. Sci., 274 (1972) 1139.
4 F. Chao, M. Costa and A. Tadjeddine, C.R. Acad. Sci., 279 (1972) 1613.
5 J.C. Canullo, W.E. Triaca and A.J. Arvia, J. Electroanal. Chem., 175 (1984) 337.
6 T. Kessler, J.C. Canullo, W.E. Triaca and A.J. Arvia, J. Electrochem. Soc., in press.
7 R. Cerviño, W.E. Triaca and A.J. Arvia, J. Electroanal. Chem., 182 (1985) 51.
8 C.L. Perdriel, W.E. Triaca and A.J. Arvia, J. Electroanal. Chem., 205 (1986) 279.
9 A.J. Arvia, J.C. Canullo, E. Custidiano, C.L. Perdriel and W.E. Triaca, Electrochim. Acta, in press.
10 J.C. Canullo, W.E. Triaca and A.J. Arvia, J. Electroanal. Chem., 200 (1986) 397.
11 E. Custidiano, A.C. Chialvo and A.J. Arvia, J. Electroanal. Chem., 196 (1985) 423.
12 R.M. Cerviño, A.J. Arvia and W. Vielstich, Surf. Sci., 154 (1985) 523.
13 E. Custidiano, T. Kessler, W.E. Triaca and A.J. Arvia, Electrochim. Acta, in press.

14 J. Gomez, L. Vázquez, A.M. Baró, N. Garcia, C.L. Perdriel, W.E. Triaca and A.J. Arvia, Nature (London), in press.
15 A. Hamelin, J. Electroanal. Chem., 165 (1984) 167.
16 A. Hamelin and J. Lipkowski, J. Electroanal. Chem., 171 (1984) 317.
17 M. Sotto, J. Electroanal. Chem., 69 (1976) 227.
18 K. Engelsmann, W.J. Lorenz and E. Schmidt, J. Electroanal. Chem., 114 (1980) 1.
19 A. Hamelin, J. Electroanal. Chem., 101 (1979) 285.
20 J.F. Nicholas in Atlas of Models of Crystal Surfaces, Gordon and Breach, New York, 1965.
21 W.S. Clabaugh, J. Res. Natl. Bur. Stand., 36 (1946) 119.
22 E.B. Sandell, Colorimetric Determination of Traces of Metals, Interscience–Wiley, New York, 1959.
23 D. Dickertmann, J.W. Schultze and K.J. Vetter, J. Electroanal. Chem., 55 (1974) 429.
24 G.J. Brug, M. Sluyters-Rehbach, J.H. Sluyters and A. Hamelin, J. Electroanal. Chem., 181 (1984) 245.
25 J.M. Feliu, J. Claret, C. Muller, J.L. Vázquez and A. Aldaz, J. Electroanal. Chem., 172 (1984) 383.
26 M.C. Galindo, M.E. Martins and A.J. Arvia, Anal. Asoc. Quim. Arg., 74 (1986) 215.
27 C.M. Ferro, A.J. Calandra and A.J. Arvia, J. Electroanal. Chem., 59 (1975) 239.
28 C.M. Ferro, A.J. Calandra and A.J. Arvia, J. Electroanal. Chem., 55 (1974) 291.
29 S.H. Cadle and S. Bruckenstein, Anal. Chem., 46 (1974) 16.
30 A.J. Rand and R. Woods, J. Electroanal. Chem., 35 (1972) 209.
31 F.E. Sanftle and D.B. Wright, J. Electrochem. Soc., 132 (1985) 129.
32 A.J. Bard, R. Parsons and J. Jordan (Eds.), Standard Potentials in Aqueous Solutions, Marcel Dekker, New York, 1985.
33 A. Hamelin, T. Vitanov, E. Sevastyanov and A. Popov, J. Electroanal. Chem., 145 (1983) 225.
34 R. Parsons, J. Electroanal. Chem., 150 (1983) 51.
35 A. Hamelin, J. Electroanal. Chem., 144 (1983) 365.
36 A. Bolzan, M.E. Martins and A.J. Arvia, J. Electroanal. Chem., 172 (1984) 221.
37 A. Hamelin, J. Electroanal. Chem., 142 (1982) 299.
38 D.G. Fedak and N.J. Gjostein, Acta Metall., 15 (1967) 827.
39 J. Perdereav, J.P. Biderian and G.E. Rhead, J. Phys. F4, (1974) 798.
40 M.A. Van Have, R.J. Koestner, P.C. Stair, J.P. Biberian, L.L. Kesmodel, I. Bartos and G.A. Somorjai, Surf. Sci., 103 (1981) 218.
41 G. Binning, H. Rohrer, Ch. Gerber and E. Weibel, Surf. Sci., 131 (1983) L379.
42 G.M. Schmid and M.E. Curley-Fiorino in A.J. Bard (Ed.), Encyclopedia of Electrochemistry of the Elements, Vol. 4, Marcel Dekker, New York and Basel, 1975, Ch. 3.